Proton and neutron electromagnetic form factors and radii from $N_f = 2 + 1$ lattice QCD

Miguel Salg, Dalibor Djukanovic, Georg von Hippel, Harvey B. Meyer, Konstantin Ottnad, Hartmut Wittig

[arXiv:2309.06590], [arXiv:2309.07491], [arXiv:2309.17232]

Lattice Seminar, HU Berlin, November 6, 2023

Outline

1. Motivation
2. Lattice setup
3. Parametrization of the Q^2-dependence
4. Model average and final results
5. Zemach radius
6. Conclusions and outlook

Outline

1 Motivation

2 Lattice setup

3 Parametrization of the Q^2-dependence

4 Model average and final results

5 Zemach radius

6 Conclusions and outlook

Proton radius puzzle: experimental situation in 2023

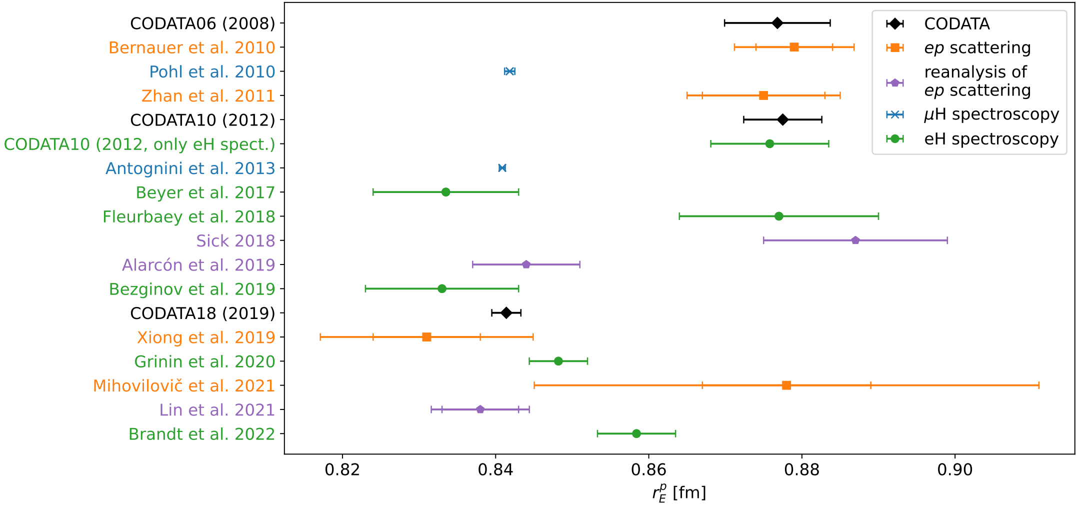

Motivation for (another) lattice study

- "Proton radius puzzle": discrepancy between different determinations of the electric and magnetic radii of the proton
- In lattice QCD as in the context of scattering experiments: radii extracted from the slope of the electromagnetic form factors at $Q^2 = 0$

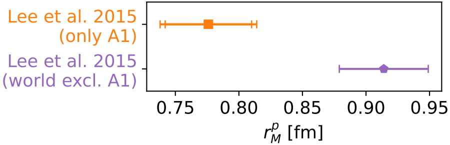

- Tension between Q^2-dependence of form factors from different experiments (A1 vs. PRad)
- Full calculation of the proton and neutron form factors from first principles necessitates explicit treatment of the numerically challenging quark-disconnected contributions
- Neglected in many previous lattice studies, in particular no simultaneous control of all relevant systematics

Outline

1. Motivation
2. Lattice setup
3. Parametrization of the Q^2-dependence
4. Model average and final results
5. Zemach radius
6. Conclusions and outlook

Ensembles

Coordinated Lattice Simulations (CLS)[1]

- Non-perturbatively $\mathcal{O}(a)$-improved Wilson fermions, $N_f = 2+1$
- $\operatorname{tr} M_q = 2m_l + m_s =$ const.
- Tree-level improved Lüscher-Weisz gauge action
- Scale setting with gradient flow time[2] $\rightarrow$ express all dimensionful quantities in units of t_0, convert to physical units with FLAG[3] $\sqrt{t_{0,\mathrm{phys}}}$

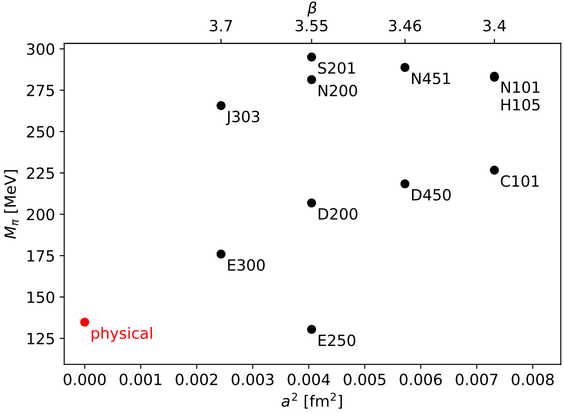

Figure: Overview of the ensembles used in this study

[1] Bruno et al. 2015 [JHEP **2015** (2), 43]; [2] Lüscher 2010 [JHEP **2010** (8), 71]; Lüscher 2014 [JHEP **2014** (3), 92]; Bruno, Korzec, and Schaefer 2017 [PRD **95**, 074504]; [3] Aoki et al. 2022 [EPJC **82**, 869].

Reweighting and vector current

- Reweight[4] all observables to compensate for the twisted mass (light quarks) and rational approximation (strange quark)
- Use the conserved vector current,

$$V_\mu^c(x) = \frac{1}{2}\left(\bar{\psi}(x+\hat{\mu}a)(\mathbb{1}+\gamma_\mu)U_\mu^\dagger(x)\psi(x) - \bar{\psi}(x)(\mathbb{1}-\gamma_\mu)U_\mu(x)\psi(x+\hat{\mu}a)\right), \qquad (1)$$

or, more precisely, the symmetrized version

$$V_\mu^{cs}(x) = \frac{1}{2}\left(V_\mu^c(x) + V_\mu^c(x-\hat{\mu}a)\right) \qquad (2)$$

- Perform $\mathcal{O}(a)$-improvement[5]
- No renormalization required

[4] Mohler and Schaefer 2020 [PRD **102**, 074506]; Kuberski 2023 [arXiv:2306.02385]; [5] Gérardin, Harris, and Meyer 2019 [PRD **99**, 014519].

Nucleon two- and three-point correlation functions

- Measure the two- and three-point correlation functions of the nucleon,

$$\left\langle C_2(\mathbf{p}'; t_{\mathrm{sep}}) \right\rangle = \sum_{\mathbf{y}} e^{-i\mathbf{p}'\cdot\mathbf{y}} \Gamma^p_{\beta\alpha} \left\langle N_\alpha(\mathbf{y}, t_{\mathrm{sep}}) \bar{N}_\beta(0) \right\rangle , \tag{3}$$

$$\left\langle C_{3,V_\mu}(\mathbf{p}', \mathbf{q}; t_{\mathrm{sep}}, t) \right\rangle = \sum_{\mathbf{y},\mathbf{z}} e^{i\mathbf{q}\cdot\mathbf{z}} e^{-i\mathbf{p}'\cdot\mathbf{y}} \Gamma^p_{\beta\alpha} \left\langle N_\alpha(\mathbf{y}, t_{\mathrm{sep}}) V_\mu(\mathbf{z}, t) \bar{N}_\beta(0) \right\rangle \tag{4}$$

- Projection matrix $\Gamma^p_j = \frac{1}{2}(\mathbb{1} + \gamma_0)(\mathbb{1} + i\gamma_5\gamma_j)$, where $(\mathbb{1} + \gamma_0)$ projects to positive parity and $(\mathbb{1} + i\gamma_5\gamma_j)$ polarizes the spin of the nucleon in j-direction
- For three-point functions, Wick contractions yield connected and disconnected contribution
- Only use $j = 3$ for connected part, average over $j = 1, 2, 3$ and over forward- and backward-propagating nucleon for disconnected part

Nucleon two- and three-point correlation functions

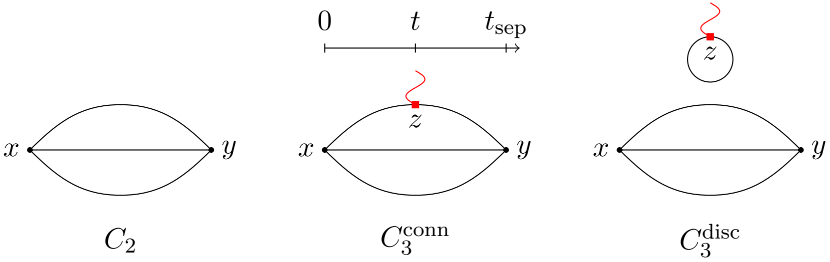

- Construct the disconnected part from the quark loops and the two-point functions,

$$\left\langle C_{3,V_\mu}^{\mathrm{disc}}(\mathbf{p}', \mathbf{q}; t_{\mathrm{sep}}, t)\right\rangle = \left\langle L^{V_\mu}(\mathbf{q}; t) C_2(\mathbf{p}'; t_{\mathrm{sep}})\right\rangle, \tag{5}$$

$$L^{V_\mu}(\mathbf{q}; z_0) = -\sum_{\mathbf{z}} e^{i\mathbf{q}\cdot\mathbf{z}}\, \mathrm{tr}[D_q^{-1}(z, z)\gamma_\mu] \tag{6}$$

From correlation functions to effective form factors

- Compute the quark loops via a stochastic estimation using a frequency-splitting technique[6]
- Generalized hopping-parameter expansion combined with hierarchical probing for one heavy flavor, one-end trick for remaining flavors
- The nucleon at the sink is at rest, *i.e.*, $\mathbf{p}' = \mathbf{0}$
- Calculate the ratios[7]

$$R_{V_\mu}(\mathbf{q}; t_{\text{sep}}, t) = \frac{C_{3,V_\mu}(\mathbf{q}; t_{\text{sep}}, t)}{C_2(\mathbf{0}; t_{\text{sep}})} \sqrt{\frac{\bar{C}_2(\mathfrak{q}; t_{\text{sep}} - t) C_2(\mathbf{0}; t) C_2(\mathbf{0}; t_{\text{sep}})}{C_2(\mathbf{0}; t_{\text{sep}} - t) \bar{C}_2(\mathfrak{q}; t) \bar{C}_2(\mathfrak{q}; t_{\text{sep}})}}, \tag{7}$$

where $t_{\text{sep}} = y_0 - x_0$, $t = z_0 - x_0$, and $\bar{C}_2(\mathfrak{q}; t_{\text{sep}}) = \sum_{\tilde{\mathbf{q}} \in \mathfrak{q}} C_2(\tilde{\mathbf{q}}; t_{\text{sep}}) \Big/ \sum_{\tilde{\mathbf{q}} \in \mathfrak{q}} 1$

[6] Giusti et al. 2019 [EPJC **79**, 586]; Cè et al. 2022 [JHEP **2022** (8), 220]; [7] Korzec et al. 2009 [PoS **066**, 139].

From correlation functions to effective form factors

- At zero sink momentum, the effective form factors can be computed from the ratios as

$$G_E^{\mathrm{eff}}(Q^2; t_{\mathrm{sep}}, t) = \sqrt{\frac{2E_{\mathbf{q}}}{M_N + E_{\mathbf{q}}}} R_{V_0}(\mathbf{q}; t_{\mathrm{sep}}, t), \tag{8}$$

$$G_M^{\mathrm{eff}}(Q^2; t_{\mathrm{sep}}, t) = \sqrt{2E_{\mathbf{q}}(M_N + E_{\mathbf{q}})} \frac{\sum_{k,l} \epsilon_{jkl} q_l \operatorname{Re} R_{V_k}^{\Gamma_j^p}(\mathbf{q}; t_{\mathrm{sep}}, t)}{\sum_{k \neq j} q_k^2} \tag{9}$$

- Build effective form factors in isospin basis, *i.e.*, $u - d$ and $u + d - 2s$
- Proton and neutron form factors defined by the combinations

$$G_{E,M}^{\mathrm{eff},p} = \frac{1}{6}\left(G_{E,M}^{\mathrm{eff},u+d-2s} + 3G_{E,M}^{\mathrm{eff},u-d}\right), \quad G_{E,M}^{\mathrm{eff},n} = \frac{1}{6}\left(G_{E,M}^{\mathrm{eff},u+d-2s} - 3G_{E,M}^{\mathrm{eff},u-d}\right) \tag{10}$$

Isovector effective form factors on E300

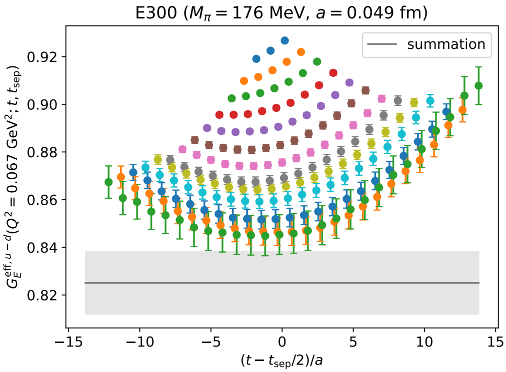

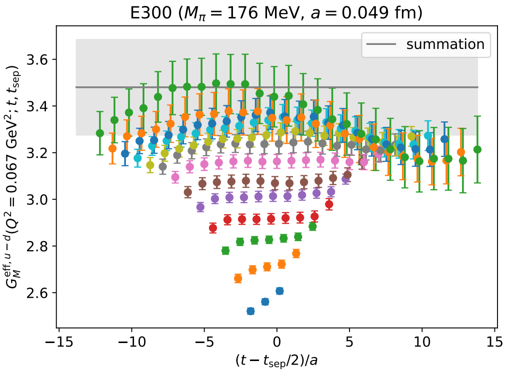

- Influence of excited-state effects clearly visible
- Errors grow drastically with t_{sep} in spite of significantly increasing statistics (more sources)

Isoscalar effective form factors on E300

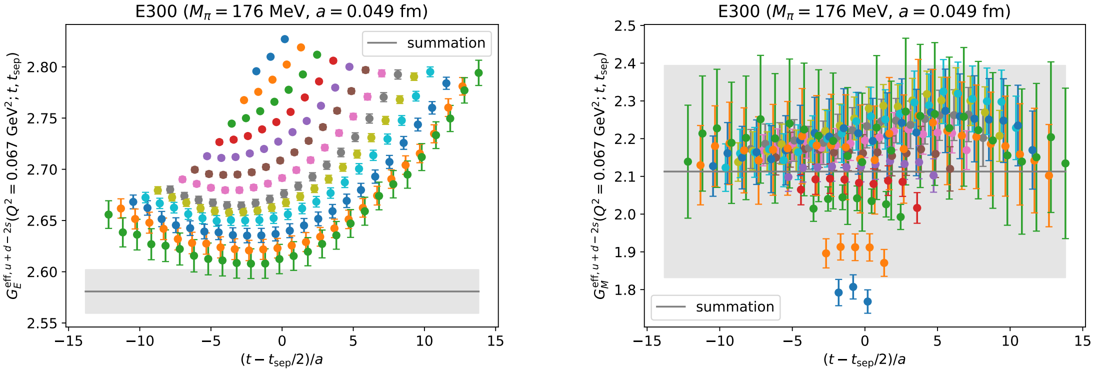

- Clear signal including disconnected contributions, errors dominated by connected part
- Contamination by excited states similar to isovector channel

Excited-state analysis: summation method

- Explicit treatment of the excited-state systematics required
- Summation of the effective form factors over the operator insertion time,

$$S_{E,M}(Q^2; t_{\rm sep}) = \sum_{t=t_{\rm skip}}^{t_{\rm sep}-t_{\rm skip}} G^{\rm eff}_{E,M}(Q^2; t, t_{\rm sep}), \quad t_{\rm skip} = 2a \tag{11}$$

- Parametrically suppresses the effects of excited states ($\propto e^{-\Delta t_{\rm sep}}$ instead of $\propto e^{-\Delta t}$, $e^{-\Delta(t_{\rm sep}-t)}$ [Δ: energy gap to lowest-lying excited state]) $\to$ "summation method"
- For $t_{\rm sep} \to \infty$, the slope as a function of $t_{\rm sep}$ is given by the ground-state form factor,

$$S_{E,M}(Q^2; t_{\rm sep}) \xrightarrow{t_{\rm sep}\to\infty} C_{E,M}(Q^2) + \frac{1}{a}(t_{\rm sep} + a - 2t_{\rm skip}) G_{E,M}(Q^2) \tag{12}$$

Excited-state analysis: window average

- Apply summation method with varying starting values $t_{\text{sep}}^{\text{min}}$ for the linear fit
- Perform a weighted average over $t_{\text{sep}}^{\text{min}}$, where the weights are given by a smooth window function[8],

$$\hat{G} = \frac{\sum_i w_i G_i}{\sum_i w_i}, \qquad w_i = \tanh \frac{t_i - t_w^{\text{low}}}{\Delta t_w} - \tanh \frac{t_i - t_w^{\text{up}}}{\Delta t_w}, \tag{13}$$

where t_i is the value of $t_{\text{sep}}^{\text{min}}$ in the i-th fit, $t_w^{\text{low}} = 0.9\,\text{fm}$, $t_w^{\text{up}} = 1.1\,\text{fm}$ and $\Delta t_w = 0.08\,\text{fm}$

[8] Djukanovic et al. 2022 [PRD **106**, 074503]; Agadjanov et al. 2023 [arXiv:2303.08741].

Excited-state analysis: window average

- Apply summation method with varying starting values $t_{\mathrm{sep}}^{\mathrm{min}}$ for the linear fit
- Perform a weighted average over $t_{\mathrm{sep}}^{\mathrm{min}}$, where the weights are given by a smooth window function[8]

E300 ($M_\pi = 176$ MeV, $a = 0.049$ fm)

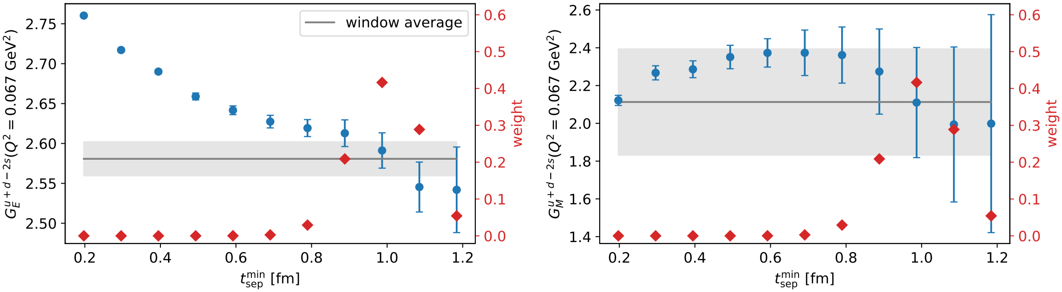

[8] Djukanovic et al. 2022 [PRD **106**, 074503]; Agadjanov et al. 2023 [arXiv:2303.08741].

Excited-state analysis: window average

D450 ($M_\pi = 218$ MeV, $a = 0.076$ fm)

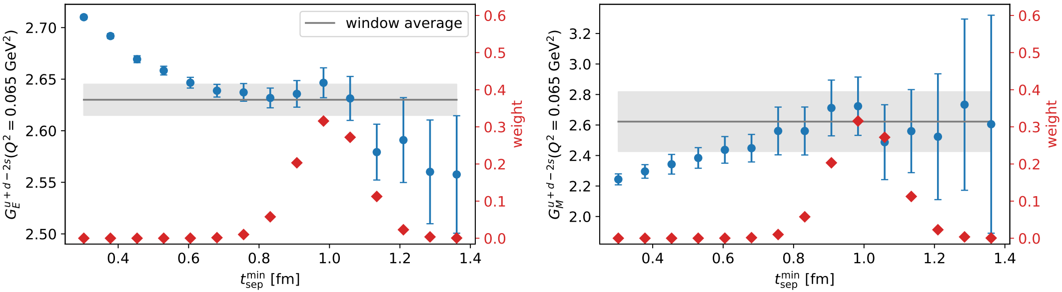

- Reliable detection of the plateau with reduced human bias (same window on all ensembles)
- Conservative error estimate

Outline

1. Motivation
2. Lattice setup
3. Parametrization of the Q^2-dependence
4. Model average and final results
5. Zemach radius
6. Conclusions and outlook

Direct Baryon χPT fits

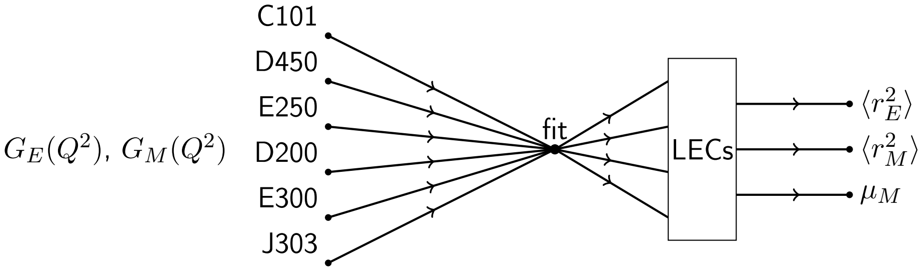

- Combine parametrization of the Q^2-dependence with the chiral, continuum, and infinite-volume extrapolation
- Simultaneous fit of the pion-mass, Q^2-, lattice-spacing, and finite-volume dependence of the form factors to the expressions resulting from covariant chiral perturbation theory[9]

[9] Bauer, Bernauer, and Scherer 2012 [PRC **86**, 065206].

Direct Baryon χPT fits: tree-level fit formulae

$$G_E^{\chi}(Q^2) = \frac{1}{2} + Q^2 \left(2d_7 + d_6\tau_3 - \frac{c_7}{4M_N} - \frac{\tilde{c}_6}{2M_N}\tau_3 + \frac{Q^2}{4M_N^2}(2d_7 + d_6\tau_3) \right) + \dots, \tag{14}$$

$$G_M^{\chi}(Q^2) = \frac{1}{2} + M_N c_7 + 2M_N \tilde{c}_6 \tau_3 + \dots, \tag{15}$$

where $\tau_3^p = +1$ and $\tau_3^n = -1$
$\Rightarrow$ terms with τ_3 only contribute for $u - d$, terms without τ_3 only for $u + d - 2s$

Direct Baryon χPT fits: tree-level fit formulae with vector mesons

$$G_E^\chi(Q^2) = \frac{1}{2} + Q^2\left(2d_7 + d_6\tau_3 - \frac{c_7}{4M_N} - \frac{\tilde{c}_6}{2M_N}\tau_3 + \frac{Q^2}{4M_N^2}(2d_7 + d_6\tau_3)\right) + \frac{M_\rho^2 + d_x g Q^2}{2(M_\rho^2 + Q^2)}\tau_3 - \frac{G_\rho Q^4}{4gM_N(M_\rho^2 + Q^2)}\tau_3 - \frac{c_\omega Q^2}{M_\omega^2 + Q^2} - \frac{c_\phi Q^2}{M_\phi^2 + Q^2} + \dots, \tag{14}$$

$$G_M^\chi(Q^2) = \frac{1}{2} + M_N c_7 + 2M_N\tilde{c}_6\tau_3 + \frac{M_\rho^2 + d_x g Q^2}{2(M_\rho + Q^2)}\tau_3 + \frac{G_\rho M_N Q^2}{g(M_\rho^2 + Q^2)}\tau_3 - \frac{c_\omega Q^2}{M_\omega^2 + Q^2} - \frac{c_\phi Q^2}{M_\phi^2 + Q^2} + \dots, \tag{15}$$

where $\tau_3^p = +1$ and $\tau_3^n = -1$
$\Rightarrow$ terms with τ_3 only contribute for $u - d$, terms without τ_3 only for $u + d - 2s$

Vector mesons in Baryon χPT

- Isospin basis: clear separation of contributing vector mesons (ρ; ω, ϕ) and all fitted LECs
- Neglect loop diagrams involving ω or ϕ mesons (numerically very small contribution)
- Reconstruct proton and neutron observables from separate fits to the isovector and isoscalar form factors
- Set mass of the ρ meson on each ensemble to the one at the corresponding pion mass and lattice spacing
- Determined from parametrization of the M_π- and a^2-dependence of the measured values of M_ρ/M_π[10],

$$\frac{M_\rho}{M_\pi} = \frac{M_{\rho,\mathrm{phys}}}{M_{\pi,\mathrm{phys}}} + A\left(\frac{1}{\sqrt{t_0}M_\pi} - \frac{1}{\sqrt{t_{0,\mathrm{phys}}}M_{\pi,\mathrm{phys}}}\right) + C(\sqrt{t_0}M_\pi - \sqrt{t_{0,\mathrm{phys}}}M_{\pi,\mathrm{phys}}) + D\frac{a^2}{t_0} \tag{16}$$

[10] Cè et al. 2022 [JHEP **2022** (8), 220].

- Set $M_\omega = M_\rho$ on each ensemble (no data for M_ω available, small mass splitting between ρ and ω)
- Employ physical ϕ mass (much heavier than ρ and ω)
- For the physical pion mass, use value in the isospin limit[11], $M_{\pi,\mathrm{phys}} = M_{\pi,\mathrm{iso}} = 134.8(3)$ MeV

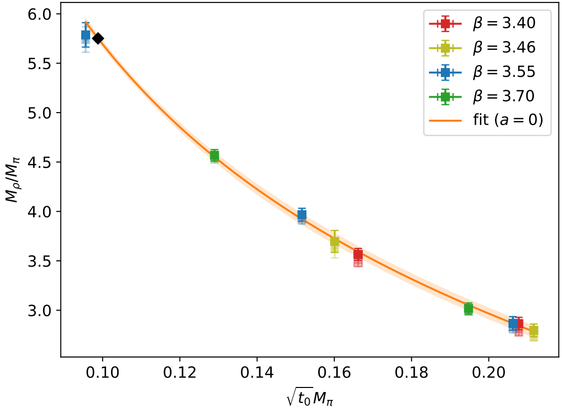

[11] Aoki et al. 2014 [EPJC **74**, 2890].

Parametrization of lattice artefacts

- Perform fits with various cuts in M_π and Q^2, as well as with different models for the lattice-spacing and finite-volume dependence, in order to estimate systematic uncertainties
- Adopt two different *ansätze* (additive or multiplicative effects),

$$G_E^{\mathrm{add}}(Q^2) = G_E^\chi(Q^2) + G_E^a a^2 Q^2 + G_E^L t_0 Q^2 e^{-M_\pi L}, \tag{17}$$

$$G_M^{\mathrm{add}}(Q^2) = G_M^\chi(Q^2) + G_M^a \frac{a^2}{t_0} + \kappa_L M_\pi \left(1 - \frac{2}{M_\pi L}\right) e^{-M_\pi L} + G_M^L t_0 Q^2 e^{-M_\pi L}, \tag{18}$$

$$G_E^{\mathrm{mult}}(Q^2) = G_E^\chi(Q^2) + \frac{G_E^a a^2 Q^2 + G_E^L t_0 Q^2 e^{-M_\pi L}}{t_0(M_\rho^2 + Q^2)}, \tag{19}$$

$$G_M^{\mathrm{mult}}(Q^2) = G_M^\chi(Q^2) + \frac{G_M^a a^2/t_0 + G_M^L t_0 Q^2 e^{-M_\pi L}}{t_0(M_\rho^2 + Q^2)} + \kappa_L M_\pi \left(1 - \frac{2}{M_\pi L}\right) e^{-M_\pi L} \tag{20}$$

Parametrization of lattice artefacts

- Finite-volume effects barely distinguishable from our data at low pion masses
- Fix κ_L to value from Heavy-Baryon χPT (HBχPT)[12],

$$\kappa_L = -\frac{M_{N,\mathrm{phys}} g_A^2}{4\pi F_\pi^2} \tau_3, \tag{21}$$

  where $\tau_3^p = +1$ and $\tau_3^n = -1 \Rightarrow \tau_3^{u-d} = +2$ and $\tau_3^{u+d-2s} = 0$
- Stabilize fits using Gaussian priors for $G_{E,M}^{a,L}$ determined from fits to ensembles at $M_\pi \approx 0.28\,$GeV alone
- No prior on G_E^a in the isovector channel (data sufficiently precise even at low pion masses)
- Major advantage of Baryon χPT fits: large number of degrees of freedom $\Rightarrow$ improved stability against lowering the Q^2-cut

[12] Beane 2004 [PRD **70**, 034507].

Q^2-dependence of the isovector form factors on E300

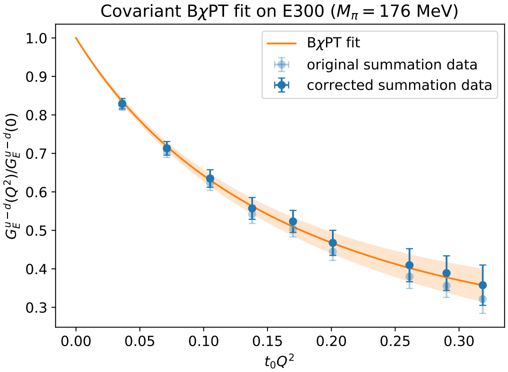

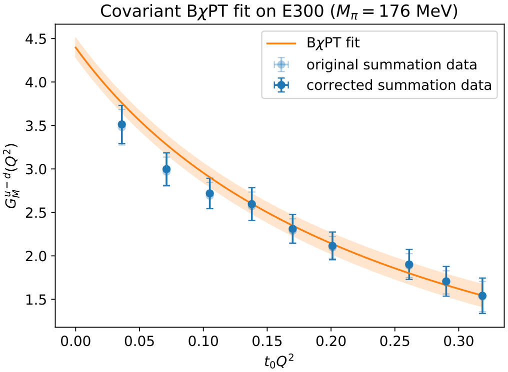

- Direct BχPT fit describes data very well
- Reduced error due to the inclusion of several ensembles in one fit

Q^2-dependence of the isoscalar form factors on E300

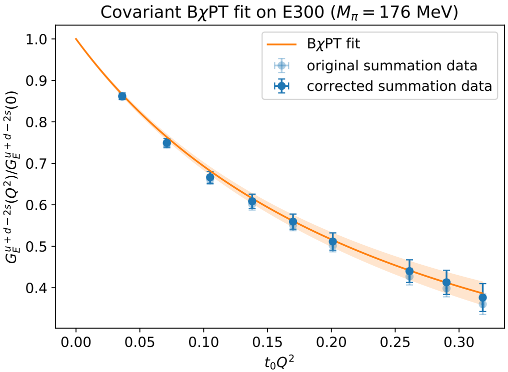

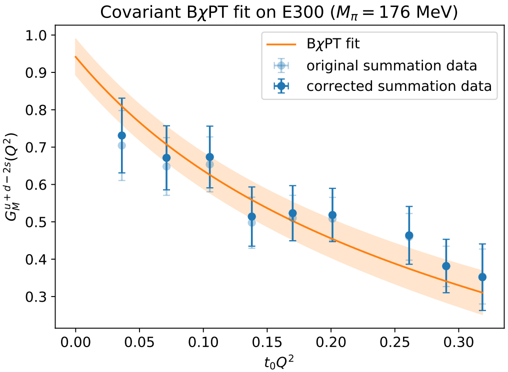

Crosscheck with z-expansion

- z-expansion[13]: model-independent description of the Q^2-dependence of the form factors on each ensemble individually
- Map domain of analyticity of the form factors onto the unit circle,

$$z(Q^2) = \frac{\sqrt{\tau_{\mathrm{cut}} + Q^2} - \sqrt{\tau_{\mathrm{cut}} - \tau_0}}{\sqrt{\tau_{\mathrm{cut}} + Q^2} + \sqrt{\tau_{\mathrm{cut}} - \tau_0}}, \tag{22}$$

  where $\tau_{\mathrm{cut}} = 4M_\pi^2$ (isoscalar: $\tau_{\mathrm{cut}} = 9M_\pi^2$), and we employ $\tau_0 = 0$
- Expand the form factors as

$$\frac{G_E(Q^2)}{G_E(0)} = \sum_{k=0}^{n} a_k z(Q^2)^k, \quad G_M(Q^2) = \sum_{k=0}^{n} b_k z(Q^2)^k \tag{23}$$

- Fix $G_E(0)$ by imposing $a_0 = 1$ (neutron: $a_0 = 0$) and truncate the expansion after $n = 2$

[13] Hill and Paz 2010 [PRD **82**, 113005].

Chiral and continuum extrapolation

- Chiral and continuum extrapolation as a second, separate step
- Employ fit formulae inspired by HBχPT[14] with leading-order pion-mass dependence,

$$\frac{\langle r_E^2 \rangle}{t_0} = A + D \ln(\sqrt{t_0} M_\pi) + E \frac{a^2}{t_0}, \tag{24}$$

$$\frac{\langle r_M^2 \rangle}{t_0} = A + \frac{D}{\sqrt{t_0} M_\pi} + E \frac{a^2}{t_0}, \tag{25}$$

$$\mu_M = A + B \sqrt{t_0} M_\pi + E \frac{a^2}{t_0} \tag{26}$$

- Isoscalar channel: one-loop terms which give rise to above pion-mass dependence don't contribute $\Rightarrow$ use simplified *ansatz* for all three observables,

$$A + C t_0 M_\pi^2 + E \frac{a^2}{t_0} \tag{27}$$

[14] Göckeler et al. 2005 [PRD **71**, 034508].

Crosscheck of direct fits with z-expansion: proton electromagnetic radii

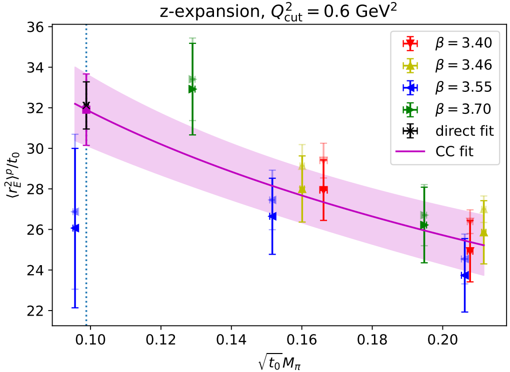

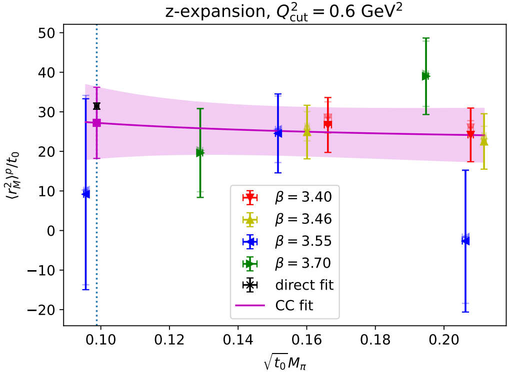

- Radii in good agreement with direct fits, albeit with significantly larger errors
- Not sufficiently stable against fluctuations on single momenta or ensembles

Crosscheck of direct fits with z-expansion: proton magnetic moment

- Magnetic moment significantly smaller than direct fits which are compatible with experiment
- Two-step process masks the relative paucity of data points at small Q^2 on some ensembles
- Direct fits use more data in one fit $\Rightarrow$ increased stability against statistical fluctuations
- Only use direct fits for final results

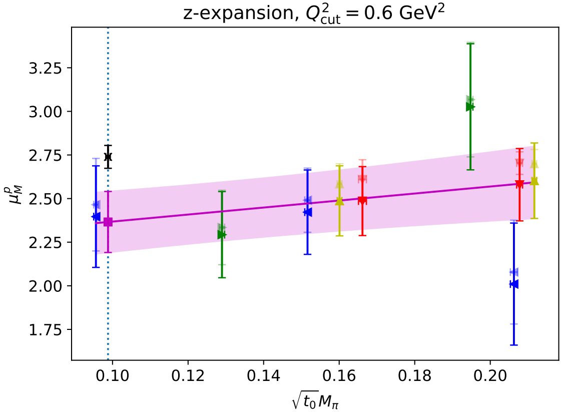

Outline

1 Motivation

2 Lattice setup

3 Parametrization of the Q^2-dependence

4 Model average and final results

5 Zemach radius

6 Conclusions and outlook

Model average

- Perform a weighted average over the results of all fit variations, using weights derived from the Akaike Information Criterion[15],

$$w_i = \exp\left(-\frac{1}{2}\mathrm{BAIC}_i\right) \Big/ \sum_j \exp\left(-\frac{1}{2}\mathrm{BAIC}_j\right) , \quad \mathrm{BAIC}_i = \chi^2_{\mathrm{noaug,min},i} + 2n_{f,i} + 2n_{c,i}, \tag{28}$$

  where n_f is the number of fit parameters and n_c the number of cut data points
- Strongly prefers fits with low n_c, *i.e.*, the least stringent cut in Q^2 $\Rightarrow$ apply a flat weight over the different Q^2-cuts to ensure strong influence of our low-momentum data
- Determine the final cumulative distribution function (CDF) from the weighted sum of the bootstrap distributions[16]
- Quote median of this CDF together with the central $68\,\%$ percentiles

---

[15] Akaike 1974 [IEEE Trans. Autom. Contr. **19**, 716]; Neil and Sitison 2022 [arXiv:2208.14983]; [16] Borsányi et al. 2021 [Nature **593**, 51].

CDFs of the electromagnetic radii and magnetic moment of the proton

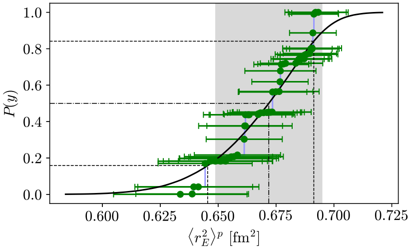

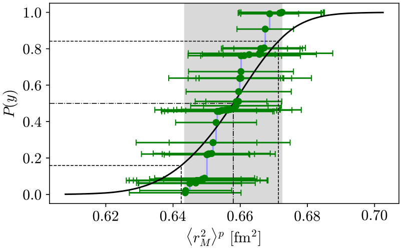

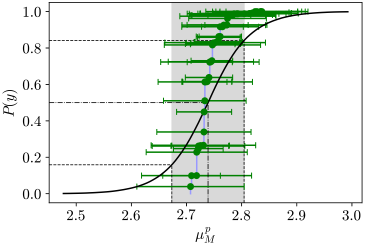

Disambiguating the statistical and systematic uncertainties

- Scale the statistical variances of the individual fit results by a factor of $\lambda = 2$
- Repeat the model averaging procedure
- Assumptions:
  - Above rescaling only affects the statistical error of the averaged result
  - Statistical and systematic errors add in quadrature
- Contributions of the statistical and systematic errors to the total error,

$$\sigma_{\mathrm{stat}}^2 = \frac{\sigma_{\mathrm{scaled}}^2 - \sigma_{\mathrm{orig}}^2}{\lambda - 1}, \qquad \sigma_{\mathrm{syst}}^2 = \frac{\lambda\sigma_{\mathrm{orig}}^2 - \sigma_{\mathrm{scaled}}^2}{\lambda - 1} \tag{29}$$

- Consistency check: results are almost independent of λ (if it is chosen not too small)

Model-averaged proton form factors at the physical point

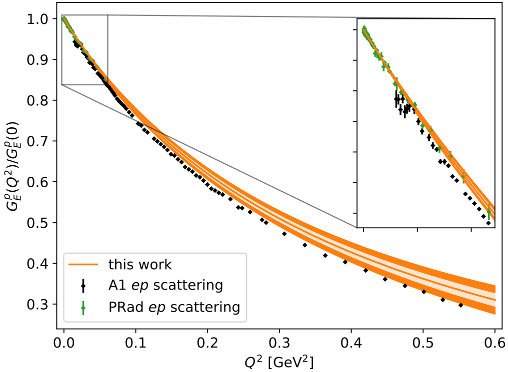

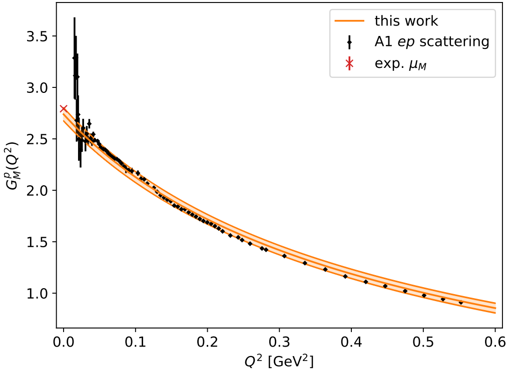

- Slope of the electric form factor closer to that of PRad[17] than to that of A1[18]
- Good agreement with A1 for the magnetic form factor

[17] Xiong et al. 2019 [Nature **575**, 147]; [18] Bernauer et al. 2014 [PRC **90**, 015206].

Model-averaged neutron form factors at the physical point

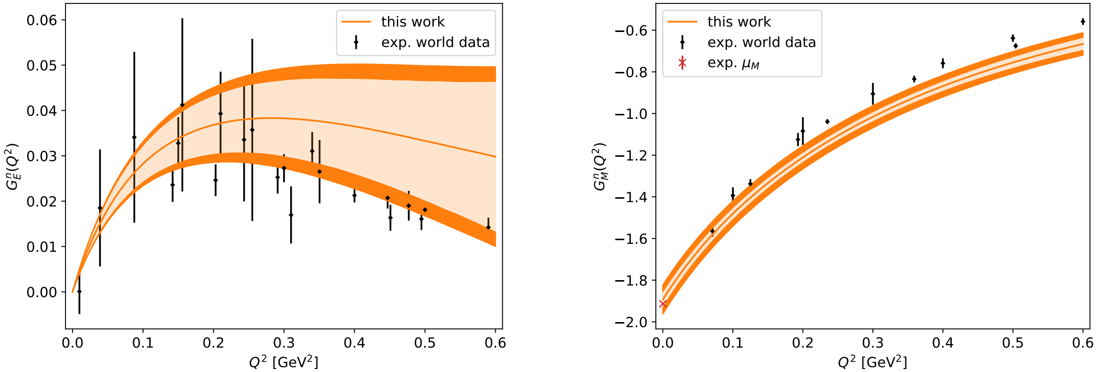

(Mostly) compatible with the collected experimental world data[19] within our errors

[19] Ye et al. 2018 [PLB **777**, 8].

Model-averaged electromagnetic radii and magnetic moments

$$\langle r_E^2 \rangle^{u-d} = (0.785 \pm 0.022 \pm 0.026)\,\mathsf{fm}^2$$
$$\langle r_M^2 \rangle^{u-d} = (0.663 \pm 0.011 \pm 0.008)\,\mathsf{fm}^2$$
$$\mu_M^{u-d} = 4.62 \pm 0.10 \pm 0.07$$

$$\langle r_E^2 \rangle^{u+d-2s} = (0.554 \pm 0.018 \pm 0.013)\,\mathsf{fm}^2$$
$$\langle r_M^2 \rangle^{u+d-2s} = (0.657 \pm 0.030 \pm 0.031)\,\mathsf{fm}^2$$
$$\mu_M^{u+d-2s} = 2.47 \pm 0.11 \pm 0.10$$

$$\langle r_E^2 \rangle^{p} = (0.672 \pm 0.014 \pm 0.018)\,\mathsf{fm}^2$$
$$\langle r_M^2 \rangle^{p} = (0.658 \pm 0.012 \pm 0.008)\,\mathsf{fm}^2$$
$$\mu_M^{p} = 2.739 \pm 0.063 \pm 0.018$$

$$\langle r_E^2 \rangle^{n} = (-0.115 \pm 0.013 \pm 0.007)\,\mathsf{fm}^2$$
$$\langle r_M^2 \rangle^{n} = (0.667 \pm 0.011 \pm 0.016)\,\mathsf{fm}^2$$
$$\mu_M^{n} = -1.893 \pm 0.039 \pm 0.058$$

Model-averaged electromagnetic radii and magnetic moments

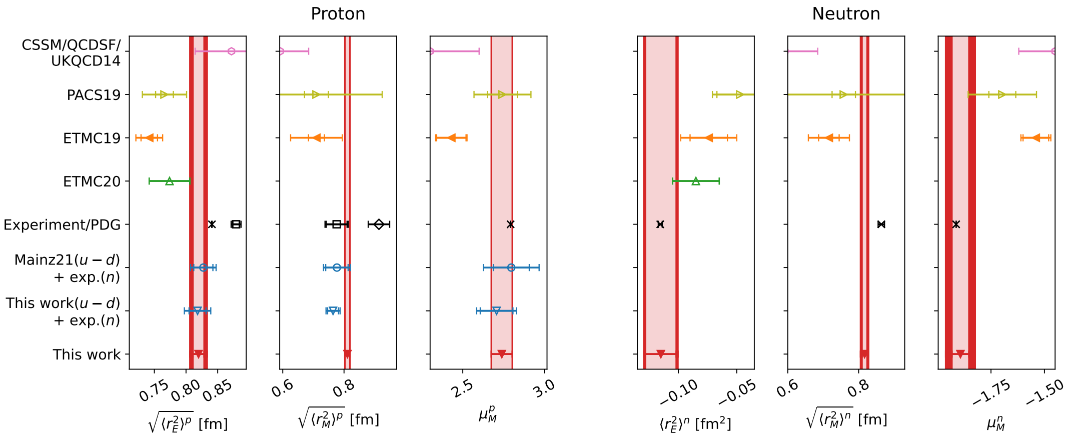

Magnetic moments reproduced, low value for $\sqrt{\langle r_E^2\rangle^p}$ clearly favored, $\sqrt{\langle r_M^2\rangle^p}$ agrees with A1

Outline

1 Motivation

2 Lattice setup

3 Parametrization of the Q^2-dependence

4 Model average and final results

5 Zemach radius

6 Conclusions and outlook

Hyperfine splitting and the Zemach radius

- Determination of nuclear properties from atomic physics
- Magnetic spin-spin interaction between the nucleus and the orbiting lepton gives rise to the hyperfine splitting (HFS)
- Electromagnetic structure of the proton influences the HFS of the S-state of hydrogen
- Relevant parameter deduced from the HFS: Zemach radius[20],

$$r_Z^p = -\frac{4}{\pi}\int_0^\infty \frac{dQ}{Q^2}\left(\frac{G_E^p(Q^2)G_M^p(Q^2)}{\mu_M^p} - 1\right) = -\frac{2}{\pi}\int_0^\infty \frac{dQ^2}{(Q^2)^{3/2}}\left(\frac{G_E^p(Q^2)G_M^p(Q^2)}{\mu_M^p} - 1\right) \tag{30}$$

- Firm theoretical prediction of the Zemach radius required both to guide the atomic spectroscopy experiments and for the interpretation of their results

[20] Zemach 1956 [Phys. Rev. **104**, 1771]; Pachucki 1996 [PRA **53**, 2092].

Zemach radius from the lattice

- BχPT including vector mesons only trustworthy for $Q^2 \lesssim 0.6\,\mathrm{GeV}^2$
- Tail of the integrand suppressed: contribution of the form factors above $0.6\,\mathrm{GeV}^2$ to r_Z less than $0.9\,\%$
- Extrapolate BχPT fit results using a z-expansion *ansatz*
- Incorporate the large-Q^2 constraints on the form factors[21] $\rightarrow$ sum rules[22]
- For integration, smoothly replace BχPT parametrization by z-exp.

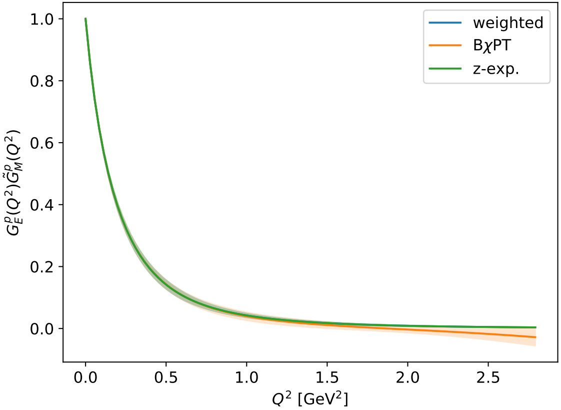

[21] Lepage and Brodsky 1980 [PRD **22**, 2157]; [22] Lee, Arrington, and Hill 2015 [PRD **92**, 013013].

Comparison to other studies

- Model-averaged result:
  $r_Z^p = 1.013(15)$ fm
  $\Rightarrow$ low value favored
- Agrees within $2\,\sigma$ with most of the experimental determinations
- Our estimate is $\sim 80\,\%$ correlated with the electromagnetic radii (based on the same form factor data)
- Low result for r_Z^p expected, no independent puzzle

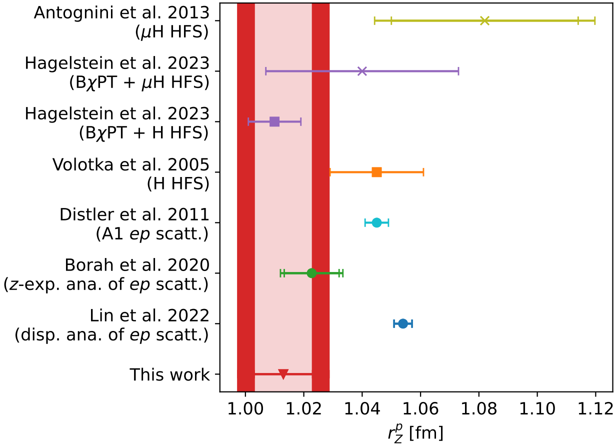

Outline

1. Motivation
2. Lattice setup
3. Parametrization of the Q^2-dependence
4. Model average and final results
5. Zemach radius
6. Conclusions and outlook

Conclusions

- Determination of the electromagnetic form factors of the proton and neutron from lattice QCD including connected and disconnected contributions, as well as a full error budget
- Chiral, continuum, and infinite-volume extrapolation via matching with the predictions from covariant baryon chiral perturbation theory
- Magnetic moments of the proton and neutron agree well with the experimental values
- Small electric *and* magnetic radii of the proton favored
- Competitive errors, in particular for the magnetic radii
- First lattice calculation of the Zemach radius of the proton $\to$ small value favored ($80\,\%$ correlation with electromagnetic radii)
- Further investigations required, in particular for the magnetic proton radius

Backup slides

Q^2-dependence of the isovector form factors on E250

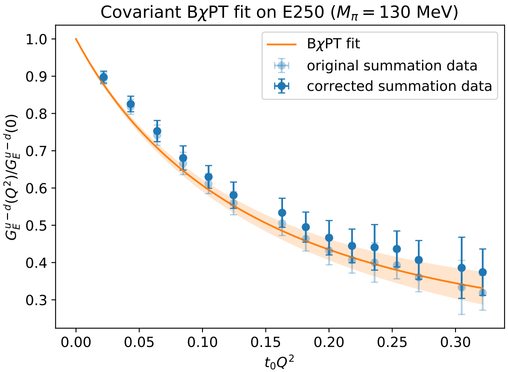

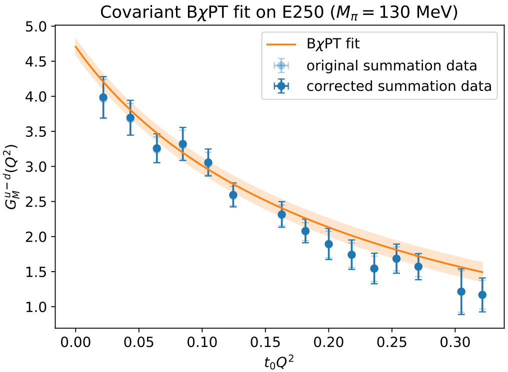

Q^2-dependence of the isoscalar form factors on E250

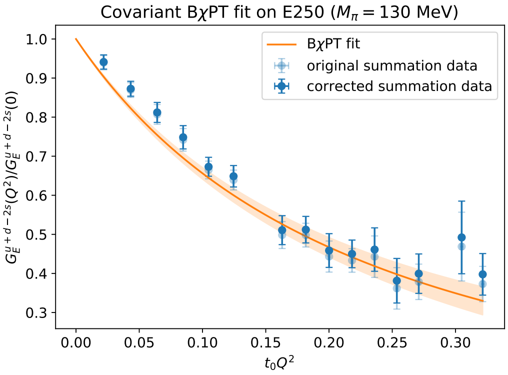

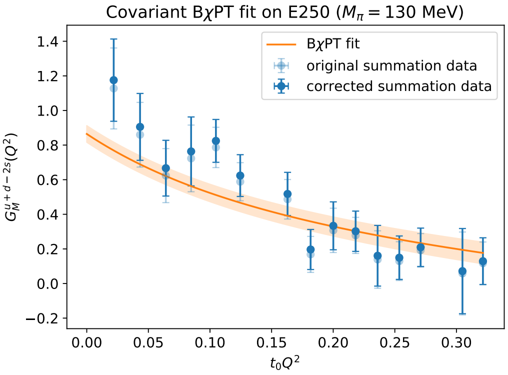

Residuals of the BχPT fits

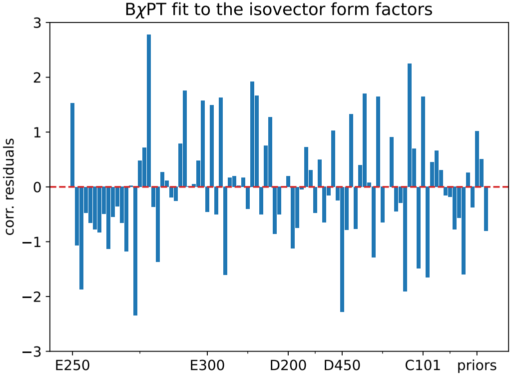

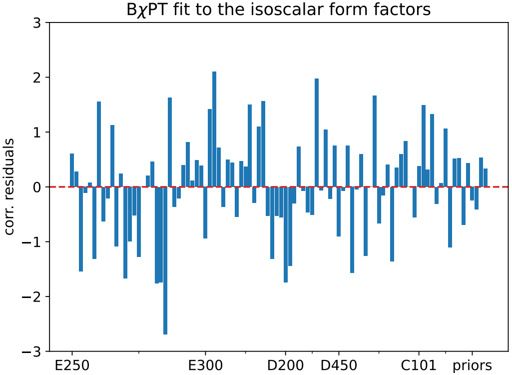

Histograms

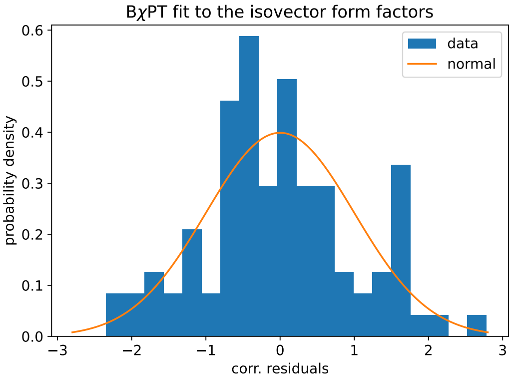

BχPT fit to the isovector form factors
data
normal
probability density
0.0
0.1
0.2
0.3
0.4
0.5
0.6
−3
−2
−1
0
1
2
3
corr. residuals

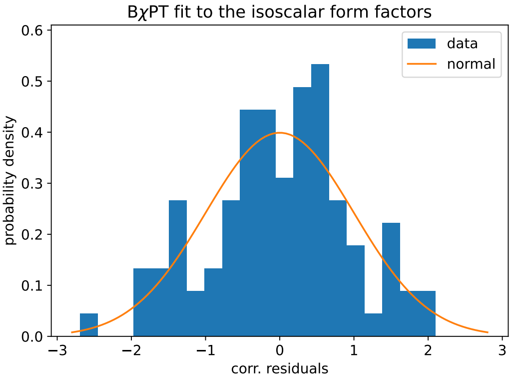

BχPT fit to the isoscalar form factors
data
normal
probability density
0.0
0.1
0.2
0.3
0.4
0.5
0.6
−3
−2
−1
0
1
2
3
corr. residuals

Q-Q plots

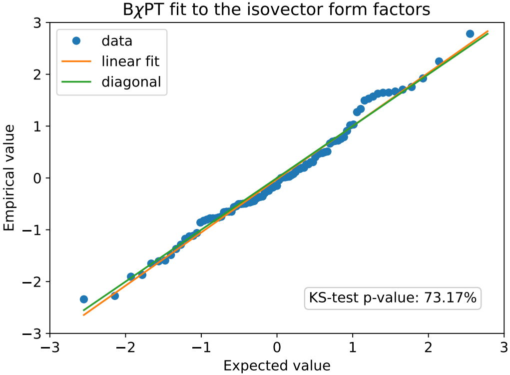
BχPT fit to the isovector form factors
data
linear fit
diagonal
KS-test p-value: 73.17%
Empirical value
Expected value
3
2
1
0
−1
−2
−3

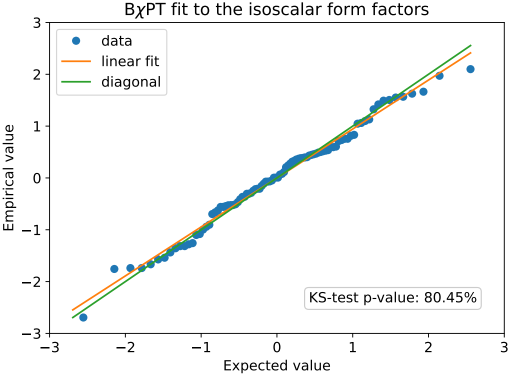
BχPT fit to the isoscalar form factors
data
linear fit
diagonal
KS-test p-value: 80.45%
Empirical value
Expected value
3
2
1
0
−1
−2
−3

Zemach integrand